SGP-TR-186

DOWNHOLE ENTHALPY MEASUREMENT IN GEOTHERMAL WELLS WITH FIBER OPTICS

Nilufer Atalay

June 2008

Financial support was provided through the
Stanford Geothermal Program under
Idaho National Engineering Laboratory Grant No. 00061418,
and by the Department of Energy Resources Engineering,
Stanford University

Stanford Geothermal Program
Interdisciplinary Research in
Engineering and Earth Sciences
STANFORD UNIVERSITY
Stanford, California

Abstract

Studies investigating ways to measure enthalpy downhole have been in progress at Stanford University for the last three years. So far, the void fraction and the dispersed-phase velocity, which are the two essential factors required for calculation of flowing enthalpy, have been determined by using resistivity and photo-sensors. Currently, research efforts have been oriented toward measuring downhole enthalpy by fiber optics.

The normal reflection probe with the tip surface cut at a right angle to the fiber axis was used to investigate the void fraction first in water-air flow then in water-steam flow. A 4-inch tall plexiglass tube was used in the experiments. The comparison measurements for void fraction were made by using the fractional flow ratio detector (FFRD). Successful results were obtained for the slow bubble flow case and water-steam flow. After void fraction measurements, a new probe with two fibers of different lengths was designed for the dispersed phase velocity measurement. The dispersed phase velocity values obtained from the fiber probe showed good agreement with the values measured by using a video camera.

After obtaining satisfactory results in the 4-inch tube, we tested our device in a 6.5-foot model wellbore and comparison measurements for void fraction were made using a resistivity sensor. The results were in good agreement. It was observed that the correlation between resistivity sensor and fiber optic sensor increased with increasing air flow rates.

Acknowledgments

I would like to express my deep and sincere gratitude to my advisor, Roland Horne. I know all the professors in Energy Resources Engineering are invaluable, but I feel myself lucky as I was in Roland's group. Throughout my study, with his enthusiasm, and his inspiration, he made everything easier for me. His wide knowledge and his logical way of thinking have been of great value for me.

Additional acknowledgements go to my colleagues, Indira, Obinna, Rob, Wenjuan, Chunmei, and Egill. I would also like to thank Kewen Li, for his guidance in the laboratory. I also must thank Joel for his cooperation in the lab.

I wish to thank my best friend, Aysegul and her husband Onur, for helping me get through the difficult times, and for being such nice neighbors, and for all the emotional support, entertainment, and caring they provided. This couple pretended as if I am from their family. Thanks!

I am indebted to Onur Can, who has helped me patiently in Ginzton Lab, his support and readiness to help made my work much smoother.

Above all, I would like to thank, my parents, Ahmet and Tanem, my sister, Yasemin and my brother, Murat for providing a loving environment for me and always being there when I need them. Special thanks go out to Yasemin, for her guidance throughout my life in America.

Finally, I owe my thanks to Fatih, his love supported me through my two-years life in Stanford. This thesis is dedicated to him.

This research was conducted with financial support through the Stanford Geothermal Program from Idaho National Engineering Laboratory, contract 00061418.

Contents

List of Tables

List of Figures

Chapter 1

1. Introduction

In geothermal reservoirs, rock is the main source of heat energy. Unlike oil and gas reservoirs in which the energy resource is the fluid itself, geothermal fluid is simply a carrier of the energy. The principle value of a geothermal reservoir to a developer lies in the thermal energy it contains; the fluid is useful only in bringing that energy to the surface. Engineered Geothermal Systems (EGS) may not contain any fluid at all – emphasizing further that the energy of the resource is only the heat contained within it.

The thermal energy contained within a substance is measured in terms of its energy content per unit mass, namely the "enthalpy". In thermodynamics, enthalpy can be defined as the thermodynamic quantity equal to the internal energy of a system plus the product of its volume and pressure. Since the energy content of the flowing geothermal fluid is one of the main concerns of the geothermal industry, measurement of enthalpy is a routine procedure during reservoir analysis. However, enthalpy is usually measured at the surface, which is not only complicated and time consuming because of the amount of equipment required but is also not necessarily equivalent to determining the enthalpy deep within the reservoir. Measuring the downhole enthalpy directly would be therefore be very valuable.

If the enthalpy can be measured in the wellbore, the measurement would not only replace the difficult surface measurement as a way of estimating reservoir energy content, it would also be possible to determine the enthalpy of specific inflow zones in the wellbore. This would be very valuable in EGS configurations, as it would enable reservoir engineers to determine which specific fractures were flowing and at what energy recovery rate.

Measuring enthalpy is also useful for:

- Reservoir modeling
- Validating results from wellbore simulators
- Earlier estimates of power produced by a well

The accurate estimation of downhole enthalpy is a significant challenge, and currently tools do not exist to make such a measurement except in single-phase flow (where the enthalpy is determinable from the temperature). To have a direct measurement of the enthalpy in two-phase flow, the temperature, pressure, void faction and mass flow rates of both phases need to be quantified. Temperature and pressure values are needed in order to find specific enthalpies of water and steam from steam tables.

Developments of optical fiber technology have brought new ways to measure pressure and temperature downhole. But there is no commercial tool for downhole enthalpy measurement and additional flow parameters (discussed in the next chapter) other than pressure and temperature are needed to determine the downhole enthalpy with fiber optics. The main idea that lies behind the downhole enthalpy measurement with fiber optics is the fiber optics' ability to detect different phases.

1.1 Previous Studies

Void fraction and dispersed-phase velocity measurement experiments with temperature, resistivity and optical sensors (composed of a phototransistor and a LED) have been carried out by Egill Juliusson, 2006. The resistivity and optical experiments have yielded successful estimates for dispersed-phase velocity and void fraction that motivated us to consider fiber optics.

Several types of optical devices have been proposed for phase detection for liquid-liquid flow or for liquid-gas flow. The most important part of the optical fiber for phase detection is its tip because refraction occurs at the probe tip. Different optical probe tip configurations have been developed for measurements in gas-liquid flows in order to

obtain total reflection when the tip is in the gas phase (Figure 1-1 shows two of them, conical tip and u-shaped tip).

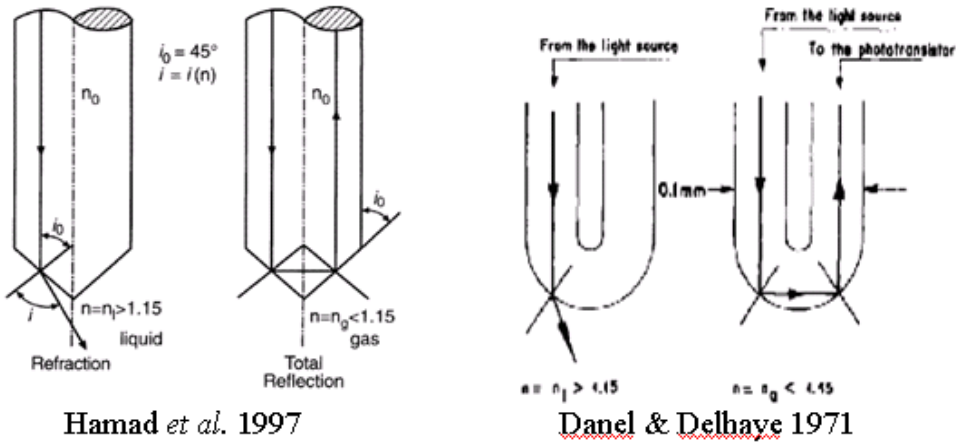

Figure 1-1: Conical and U-shaped fiber tips to obtain total reflection in gas phase.

In our study, we used a normal reflection probe with the tip surface cut at a right angle to the fiber axis, in other words the fiber tip was flat. Two investigations of gas-liquid flows and one liquid-liquid flow with this probe type have been described by Sekoguchi *et al.* 1984, Morris *et al.* 1987 and Hamad *et al.* 1997. The current investigation used the normal cut optical probe in gas-liquid flow for high temperature (water-steam flow) void fraction determination and dispersed phase velocity measurement.

Optical probe developments have been described in a review paper by Cartellier and Achard (1991) and the working principles of optical probes will be explained in the next chapter.

Chapter 2

2. Theory

2.1. In-Place and Flowing Enthalpy

Enthalpy can be defined as follows:

$$h = U + pv \tag{2.1}$$

where h is the heat energy content per unit mass, U is the internal energy per unit mass, p is the pressure and v is the specific volume.

In geothermal wells at saturated conditions, in-place enthalpy and flowing enthalpy can be calculated as follows:

In-place enthalpy:

$$h_{static} = xh_s + (1-x)h_w \tag{2.2}$$

Flowing enthalpy:

$$h_{flowing} = \frac{W_w h_w + W_s h_s}{W_w + W_s} \tag{2.3}$$

Where x is the mass fraction between steam and water, h_s and h_w are specific enthalpies of steam and water (they can be found from steam tables with T and p data), W_w and W_s are mass flow rates of water and steam ($W = q * \rho$). What we are interested in is the determination of flowing downhole enthalpy; therefore we will focus on Equation (2.3):

If the void fraction (α) of a two-phase fluid is known then the volumetric flow rate of each phase can be calculated as follows:

$$q_{gas} = u_{gas} * A * \alpha \tag{2.4}$$

$$q_{liquid} = u_{liquid} * A * (1 - \alpha) \tag{2.5}$$

Then, by using the volumetric flow rate equations, Equation (2.3) can be rewritten as follows:

$$h_{flowing} = \frac{\left[u_l * (1-\alpha) * \rho_l * h_l\right] + \left[u_g * \alpha * \rho_g * h_g\right]}{u_l * (1-\alpha) * \rho_l + u_g * \alpha * \rho_g} \tag{2.6}$$

As it can be seen from Equation (2.6), the velocities of each phase and the void fraction are the main parameters that we need to measure in order to determine the downhole enthalpy. There are several well-known methods that can be used for continuous phase velocity measurements in two-phase flow, like hot-film anemometry. Therefore, in this study we concentrated on measuring only void fraction and the dispersed-phase velocity.

2.2. Flow Parameters Needed to Determine Downhole Enthalpy

2.2.1. Void Fraction

In our study the main property to measure is the void fraction, which is a direct measurement of the relative time the dispersed phase is present at the measuring point.

Using the definition given by Hamad et al. (1997) the local void fraction can be measured by using the dispersed-phase density function $M(x,t')$ defined as

$$M(x,t') = \begin{cases} 1 & \text{If x is in the dispersed phase at time t} \\ 2 & \text{otherwise.} \end{cases} \tag{2.7}$$

For statistically stationary conditions the local void fraction $\alpha = \alpha(x)$ can be defined by

$$\alpha(x,t) = \frac{1}{T} \int_{t-T/2}^{t+T/2} M(x,t')dt' \tag{2.8}$$

Alternatively the local void fraction can also be determined by a time-averaging procedure as

$$\alpha(x) = \lim_{T-->\infty}(\sum T_G / T) \tag{2.9}$$

where T is the total measurement time and $\sum T_G$ is the total time the dispersed phase was present at the selected measuring point. In our experiments, for the determination of $\alpha(x)$, Equation (2.9) is used.

2.2.2. Dispersed-Phase Velocity

The dispersed phase velocity is another quantity that is closely related to the estimation of enthalpy. A common and effective method of measuring dispersed-phase velocity using gas-liquid discrimination sensor is to measure signals at two separate locations along the same stream line.

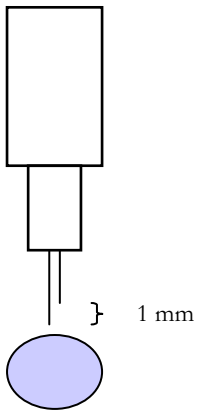

Figure 2-1: A bubble approaching to a dual-optical probe.

The distance between the sensors (Δx) should be kept small and, by using the time difference corresponding to the passing of the front of a bubble past the two sensors, the velocities of individual bubbles could be evaluated from the velocity equation:

$$u_g = \frac{\Delta x}{\Delta t} \tag{2.10}$$

Then the dispersed phase velocity was obtained by averaging the individual bubble velocities in each test run. Equation 2.10 was used to calculate bubble velocity when a few bubbles existed in the test run. However it was hard to calculate each bubbles' velocity when there existed a lot of bubbles in the test run, therefore in that case we used

the cross-correlation technique. The cross correlation technique allows one to determine the mean transit time of a flowing medium passing two sensors located a given distance apart. Hence an average velocity can be obtained as the ratio of the sensor separation Δx to transit time Δt as in Equation (2.10). This method has been applied to bubble velocity evaluation with dual optical probes (Moujaes and Dougall 1987, Saberi *et al.* 1995).

In this method, the bubble velocity was obtained by the cross correlation technique applied to the two signals $S_1(t)$ and $S_2(t)$ from the two fibers giving the following correlation $R(\tau)$:

$$R(\tau) = \frac{1}{T}\int_0^T S_1(t) * S_2(t+\tau)dt \qquad (2.11)$$

where T is the total test duration and the transit time used in our velocity equation was the τ value that gave us the maximum correlation $R(\tau)$.

2.3. Fiber Optics for Phase Detection

It is now well known that optical techniques can be used for phase detection. Such techniques are usually based on Snell's law and take advantage of the fact that the indices of refraction of the liquid and vapor phases are quite different.

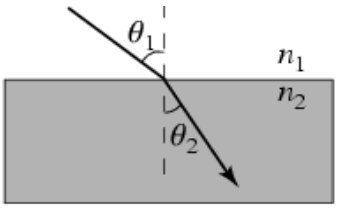

Figure 2-2: Refraction of light at an interface between two materials.

Snell's law gives the relationship between angles of incidence and refraction for a wave impinging on an interface between two media with different indices of refraction. The law follows from the boundary condition that a wave is continuous across a boundary, which requires that the phase of the wave be constant on any given plane, resulting in:

$$n_1 \sin\theta_1 = n_2 \sin\theta_2 \qquad (2.12)$$

where θ_1 and θ_2 are the angles from the normal of the incident and refracted waves, respectively.

Depending on the refraction index of the medium in which the fiber optic probes are placed, more or less of the emitted light returns to the receiving fiber. When placed in water, most of the light leaves the fiber and is dispersed in the water, while when immersed in air most of the light is refracted back into the receiving fiber.

Different configurations of optical probes have been reported for phase detection, most of them were based on the Snell-Descartes refraction law and they had a restriction on the phase index of the flowing mixture.

In a second configuration, the normal reflection probe with the tip surface cut at a right angle to the fiber axis has no restriction on the indices of the flowing mixture. As mentioned earlier, two investigations of gas-liquid flows and one liquid-liquid flow with this probe type have been described by Sekoguchi *et al.* 1984, Morris *et al.* 1987 and Hamad *et al.* 1997. The current investigation is the first study that used the normal cut fiber optic probe in water-steam flow.

The principle of this probe is based on the variation in the reflection coefficient (the Fresnel coefficient) at the probe tip with the index of each fluid (Morris *et al.* 1987). The Fresnel coefficient R for a normal light incidence at the interface between the fiber and the surrounding fluid is:

$$R = \left(\frac{n_0 - n}{n_0 + n} \right)^2 \qquad (2.13)$$

Chapter 3

3. Experiments

In this research project experiments testing the applicability of using fiber optics to measure local void fraction and dispersed-phase velocity in a two phase (liquid-gas) flow were carried out. Initially, tests were performed in a 1 ¼ inch inner diameter plexiglass tube as shown in Figure 3-1, both water-air and water-steam flows were tested in that small tube. Then we tested our sensor in a model plexiglass wellbore (Figure 3-1) which is 6.5 ft tall and 5.5 inch in inner diameter, water-air flow was used during the tests in the model wellbore.

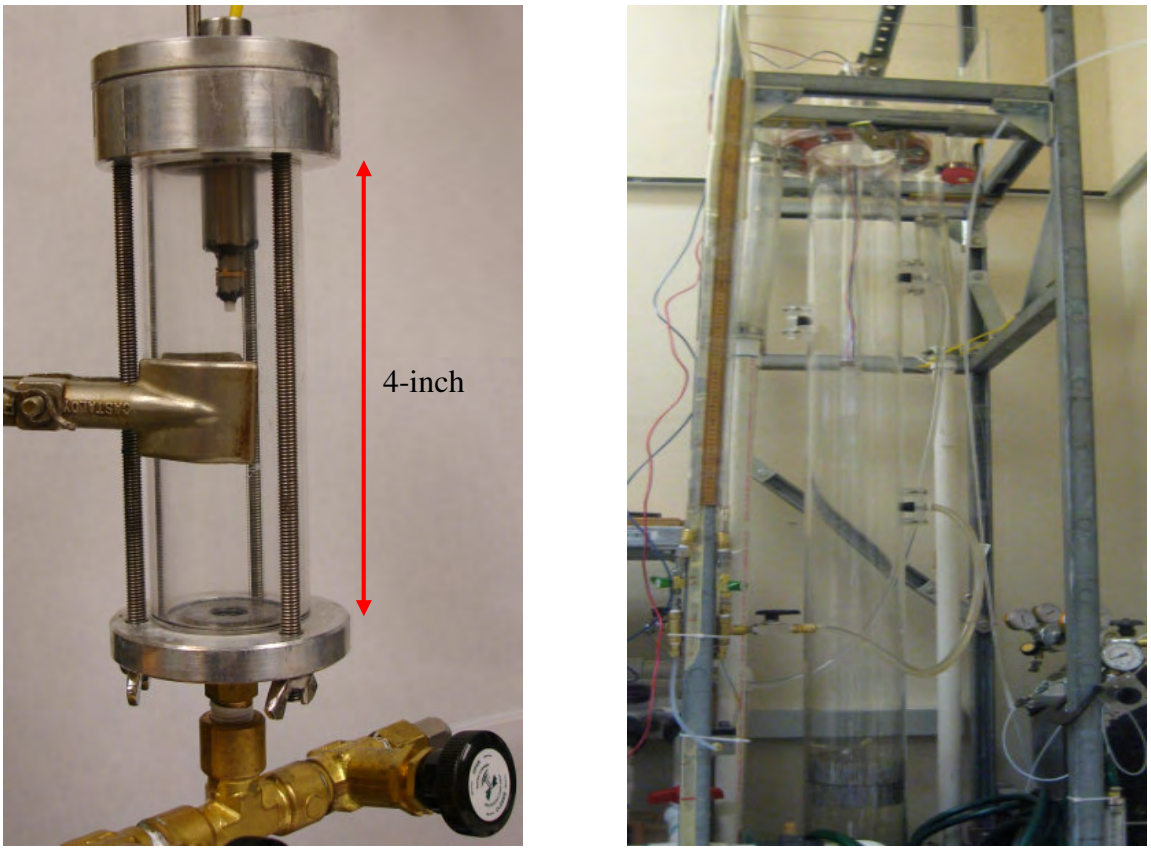

Figure 3-1: Photographs of the 4-inch test tube and the 6.5 ft model wellbore.

3.1. Fiber Position

Initially the applicability of using horizontal or vertical fiber tips was investigated. For this purpose, a horizontal and a vertical fiber tip were placed as close as possible to each other as seen in Figure 3-2 this ensures that they can detect the same bubble at the same time.

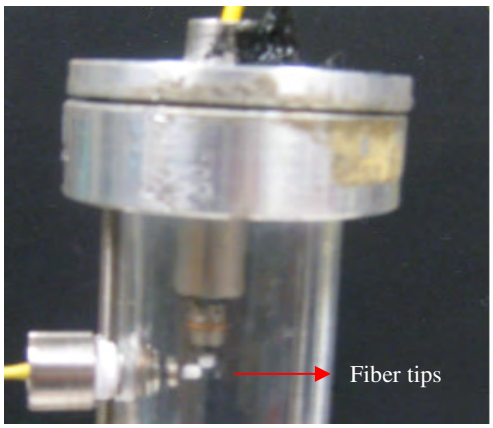

Figure 3-2: Placement of fiber tips.

A vertical fiber tip was found to be more efficient than the horizontal one since it detected more bubbles. Hence, we pursued our experiments by using the vertical fiber tip.

3.2. Experimental Apparatus

The optical monomode fiber with a normal cut fiber tip was placed inside a stainless steel tube, which was used to hold the fiber rigid. The steel tube was inserted vertically inside a plexiglass tube that was 4 inch in length and had 1¼ inch ID. A schematic diagram of the experiment is shown in Figure 3-3. A Fiber Optic Laser Diode Source (FOSS-01-3S-9/125-1310-S-1 from Ozoptics) with 1310 nm wavelength, 1 mW output, for 9/125µm core/cladding, single mode fiber, with super FC/PC receptacle was used to send invisible light to the fiber tip.

The light was transmitted through a 1x2 single mode coupler (F-CPL-S12151 from Newport Electronics). Input light was sent to the probe tip and 90% of the light reflected at the tip was coupled back to a detector (D400FC InGaAs from Thorlabs) placed on the other side of the coupler. Different amount of light was reflected back depending on the

phase around the tip. The light signal coming from the coupler was converted into voltage signal and also amplified inside the detector.

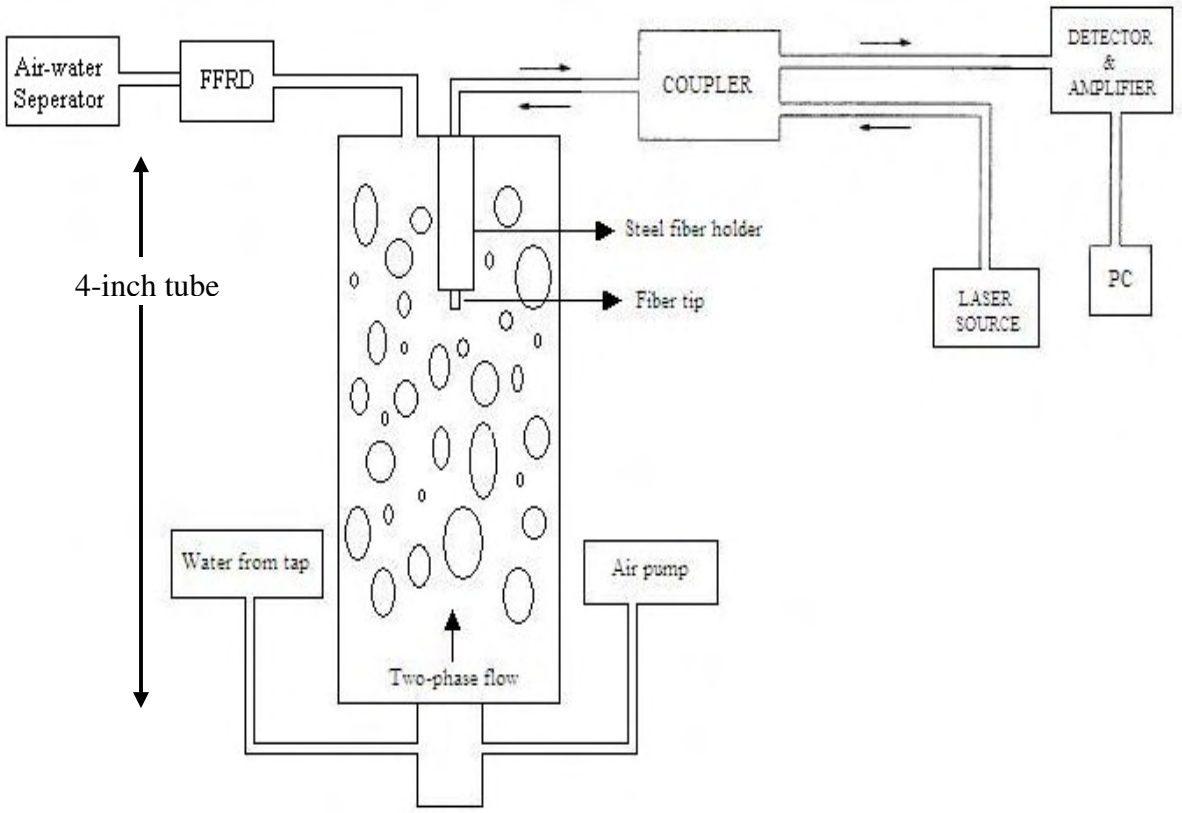

Figure 3-3: Schematic of experimental apparatus.

The whole system was connected to a computer through a data acquisition system. The terminal block and data acquisition card used were SCB-68 and NI-6281, respectively. LabView 8.2 was used to digitize the voltage signals; the VI used was "Cont Acq&Graph Voltage-Write Data to File (TDMS).vi" which is one of the sample VIs available in the LabView 8.2 software. The program recorded the signals simultaneously at 1 kHz and output the results to a scaled TDMS file for further data processing.

More light was reflected when the tip was inside the gas phase and the fiber tip only detected the bubbles that touched its surface.

After water-air test runs, the air tube was removed and water was heated by a coil and two gas burners as seen in Figure 3-4 to obtain water-steam flow.

Figure 3-4: Water-steam supplier

A Fractional Flow Ratio Detector (FFRD) (Figure 3-5) similar to that developed by Chen et al. (2004) was used at the exit of the tube for comparison measurements during void fraction tests. Detailed information about the FFRD is given in the next section.

3.3. Comparison Measurement Techniques

3.3.1. Fractional Flow Ratio Detector

The FFRD (Figure 3-5) is a simple tool composed of a LED and a phototransistor on the opposite sides of a thin transparent tube. Different voltages were produced by the phototransistor inside the FFRD when sensing different strengths of light. As mentioned in the previous section, the FFRD was used as a second method to measure void fraction, and local void fraction results obtained from the fiber probe were compared with the FFRD results.

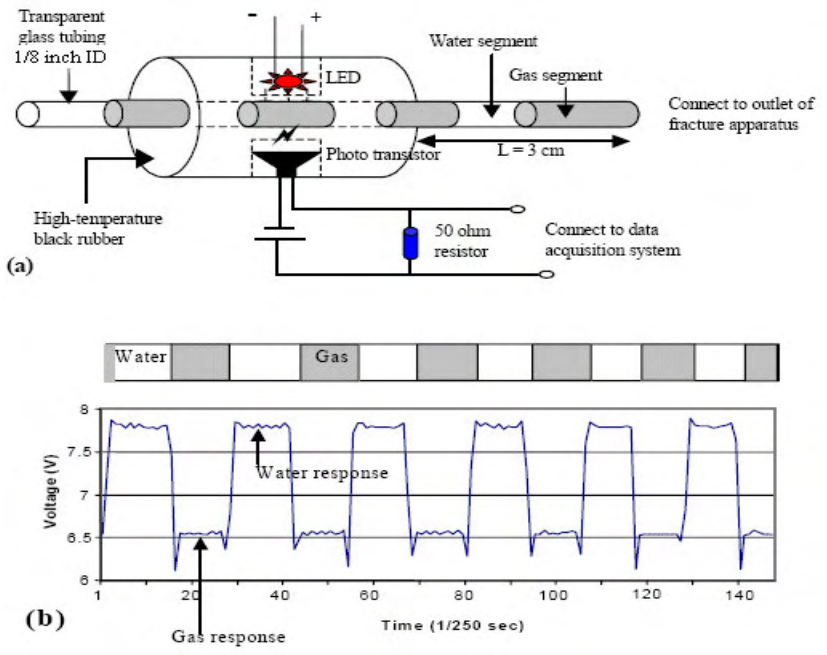

Figure 3-5: Fractional flow ratio detector (FFRD) (a) schematic (b) detected gas and water signal corresponding to different gas and water segments inside FFRD tubing, from, Chen *et al*. (2004).

3.3.2. Camera

To check the accuracy of the dual optical probe for dispersed phase velocity measurements we used images recorded by a video camera (Sony DCR-TRV140) and processed using Pinnacle Studio software (PSS). PSS could divide 1 second of video into 30 frames, which means the duration between the two consecutive frames is 33.3 millisecond.

Depending on the flow rate of the gas phase, we could visually detect the distance that the bubble travels within 33.3 ms (Figure 3-6). Hence, a bubble's velocity was calculated by using the simple velocity equation:

$$u_b = \frac{\Delta x}{33.3} \tag{3-1}$$

This camera method was used to calculate each bubble's velocity in a test run, when the gas phase flow rate was slow enough to detect the bubbles visually.

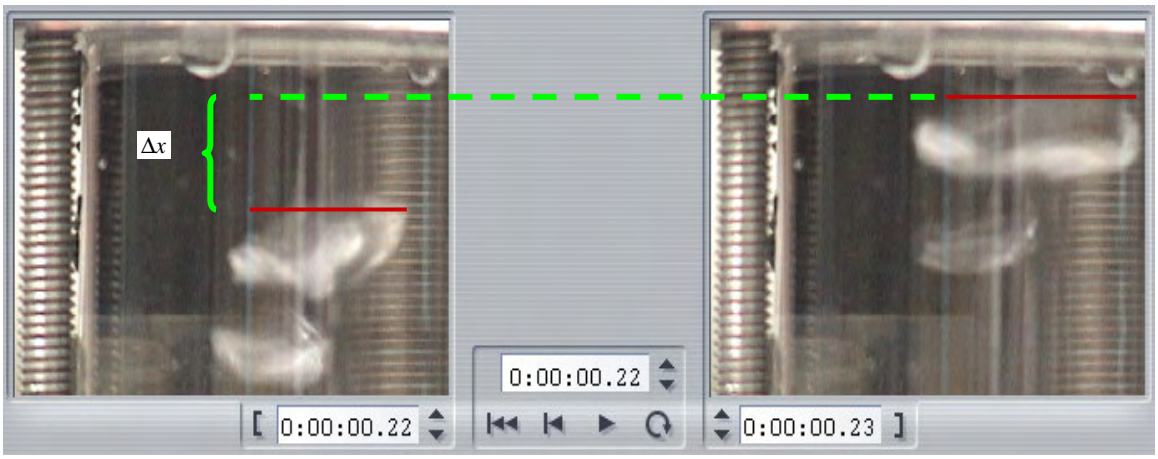

Figure 3-6: A view of two consecutive frames that shows the distance that a bubble travels within 3.33 ms.

Then the calculated bubble velocities were averaged to obtain the average dispersed-phase velocity for that test run.

3.3.3. Resistivity Sensor

Based on the earlier study by Juliusson (2006), resistivity measurements were considered to be a useful way to obtain a second set of measurements for comparison with those from the fibers. The resistivity sensors described here were constructed by coworker Joel Sandler.

Void fraction and dispersed phase velocity measurements were conducted first in a 4-inch plexiglass tube and then in a 6.5 ft model wellbore. During the void fraction measurements within the model wellbore, a resistivity sensor was used for comparison. Percent air-water values were measured using the voltage drop across an electrode in dispersed air-water flow. Proper setup proved critical in obtaining valid data in this experiment. As such, several configurations were considered and tested in both an artificial well and a small glass column in order to optimize the signal to noise ratio. After obtaining the optimum sensor design, several runs were made to find resistivity-inferred and fiber-inferred void fraction values for four different air-flow rates.

3.3.3.1. Resistivity Sensor Design

Three sensor designs were considered in this experiment. All sensors were mounted around a 1.25 inch diameter plexiglass tube that was lowered into the flow as can be seen in Figure 3-7. The first, designed by Egill Juliusson, consisted of two flat copper plates bent around the inner tube. Another design was a horizontal one inspired by Paul Spielman's four electrode setup (Spielman, 2003). Four electrodes (two for measuring voltage and two for applying a voltage, by Spielman's design) were equally spaced horizontally along the front half of the inner column. The electrodes themselves were made of solid-core copper wire and extended about half an inch from the base of the tube. The last design similarly consists of four electrodes but here they were vertically aligned along the front half on the inner tube and separated by only about 2mm.

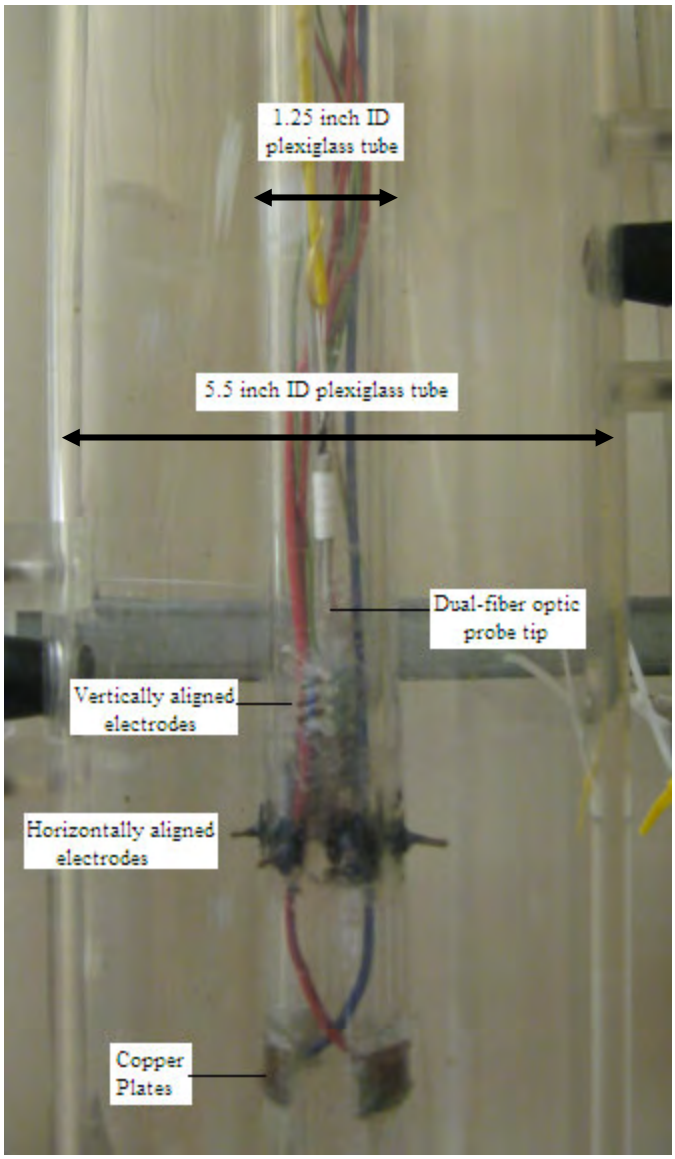

Figure 3-7: Three different resistivity sensor designs; with vertically aligned electrodes, horizontally aligned electrodes and copper plates.

3.3.3.2. Model Wellbore Test Loop

Like the resistivity sensor, fiber optic probe was also attached to the outer part of 1.25 inch plexiglass tube that was lowered into the flow. Besides the sensors, the large test loop consisted of an artificial well column, piping, pump, flow measurement equipment, pressure gauges, and the air-water source (Figure 3-8). This flow loop was designed and constructed originally by Kumar (1995).

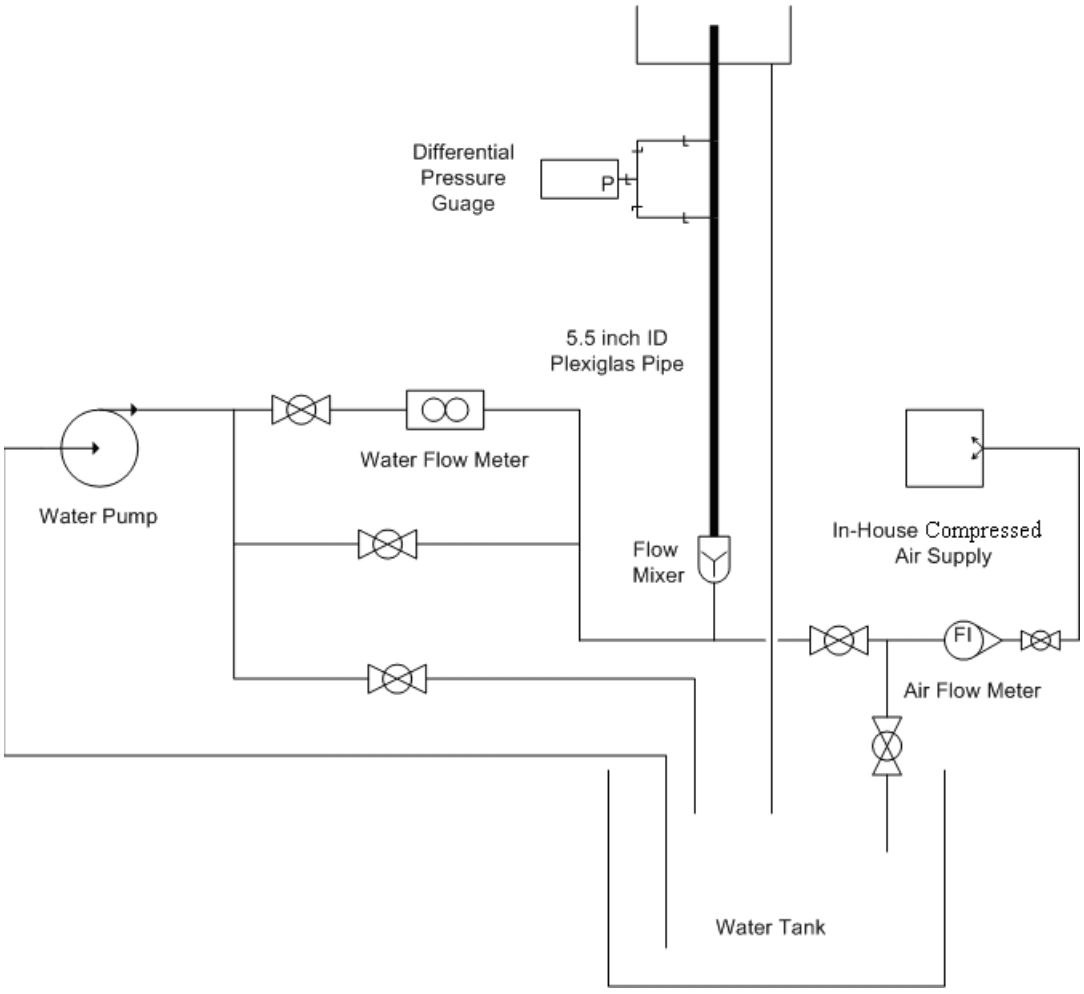

Figure 3-8: A schematic diagram of the flow loop used to test resistivity and fiber optic sensors.

The artificial well column was made of plexiglass, 5.5 inches in inner diameter, and 6.5 feet tall. At the bottom of the column, two diffusers were situated to provide a homogenous flow. While this helped better simulate well conditions, the diffusers made visually identifying individual bubble signals more difficult. Water was circulated using 1.5 inch diameter PVC piping. The electric pump was capable of pumping 150 lb/min (~2.40 cu ft/min). Although the apparatus included a digital flow meter (for the water), pressure transducers along the test column, and an air rotameter for comparison with void fraction measurements, these were not utilized in this experiment. Compressed air was supplied via an in-house air system, capable of supplying up to 5 SCFM (standard cubic feet per minute).

Chapter 4

4. Data Analysis and Results

4.1. Results of the Experiments in 4-inch Tube

4.1.1. Local Void Fraction Results

Local void fraction measurements were conducted with a single fiber for slow and fast bubble flows (water-air) and then for water-steam flow. We used the time averaging procedure to calculate the local void fraction (Equation 2-9).

In order to reduce the noise in our data we drew a threshold line and all the values above the threshold line were set to one (gas-phase) and those below were set to zero (liquid-phase). The threshold line varied in time based on the local variations in the signal. One advantage of using a method like this was that it might be useful in situations where the properties of the fluid are changing in time (e.g. if the measurement tool is being used downhole, the resistivity of the fluid would vary with temperature and salinity). Figure 4-1 shows a typical signal that we obtained from the water-air flow.

Successful results were obtained when the water-air flow was slow (Figure 4-2-a), however a good 1:1 correlation could not be obtained for the fast water-air flow because of the poor results obtained from the FFRD. Hence, this does not mean that fiber probe did not work well for fast flow rates (only that the FFRD did not).

In water-steam tests, the cross plot between the two measurements (FFRD and the fiber probe) followed the 1:1 line closely (Figure 4-2-b). During water-steam flow, although the flow was quite fast, a good correlation was obtained because some of the steam bubbles condensed while they were passing through the FFRD tube.

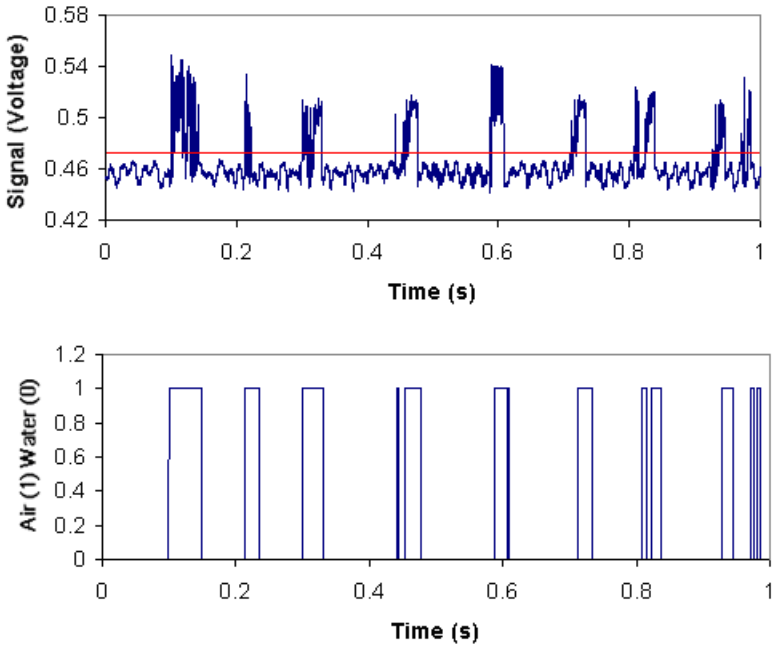

Figure 4-1: Typical voltage signal obtained before and after the threshold line was drawn.

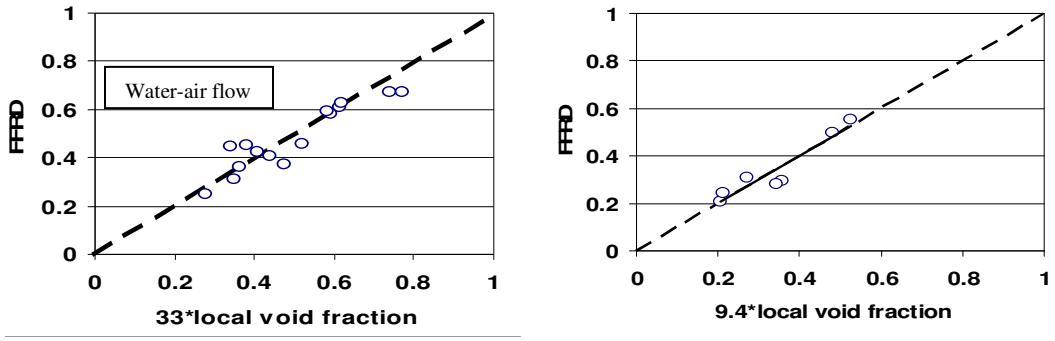

Figure 4-2: a) Relationship between FFRD-inferred and fiber-inferred void fraction values for slow bubble flow. b) Relationship between FFRD-inferred and fiber-inferred void fraction values for water-steam flow.

4.1.2. Dispersed Phase Velocity Results

Secondly, dispersed phase velocity measurements were performed with a dual optical probe. The main concern with the dual optical probe was obtaining the optimum distance between the two fibers. Different configurations were tried in order to determine the optimum distance. It was observed that the signals obtained from the trailing fiber were poor when the fibers were close (~0.1 mm apart) or when they were in contact with each other. The optimum configuration of two fibers was determined to be 1 mm and 0.5 mm

for vertical and horizontal separations, respectively. Figure 4-3, shows typical signal that was obtained during the passage of a bubble through the dual optical probe. The time it takes a bubble to travel from the leading sensor tip to the trailing sensor tip is marked with a green arrow. A single bubble's velocity can be calculated as in Equation (2.10) where $\Delta x = 1$ mm and $\Delta t = t_2 - t_1$.

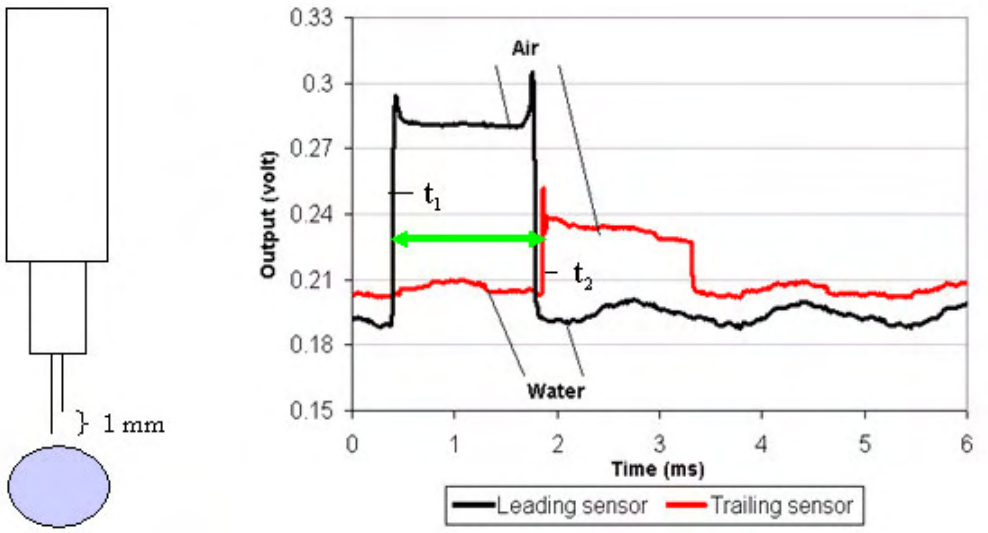

Figure 4-3: Dual optical probe signal corresponding to a single bubble passing the probe.

However, it was not possible to determine the average dispersed phase velocity from a single bubble because the difference between t_2 and t_1 changes according to bubble size, shape and striking locations. Figure 4-4 shows the dual optical probe response when striking a bubble from different points, i.e. centrally, off centre. In this figure, Δt values represent the residence times of the optical fibers inside the bubble and green arrows show the travel time of the bubble from the leading sensor tip to the trailing sensor tip. Because of these differences between individual bubbles, the dispersed-phase velocity was found either by averaging or by using the cross correlation technique described in Equation (2.11). In cross correlation method, the dispersed phase velocity was evaluated from the value of τ which gives the maximum value for $R(\tau)$ as shown in Figure 4-5.

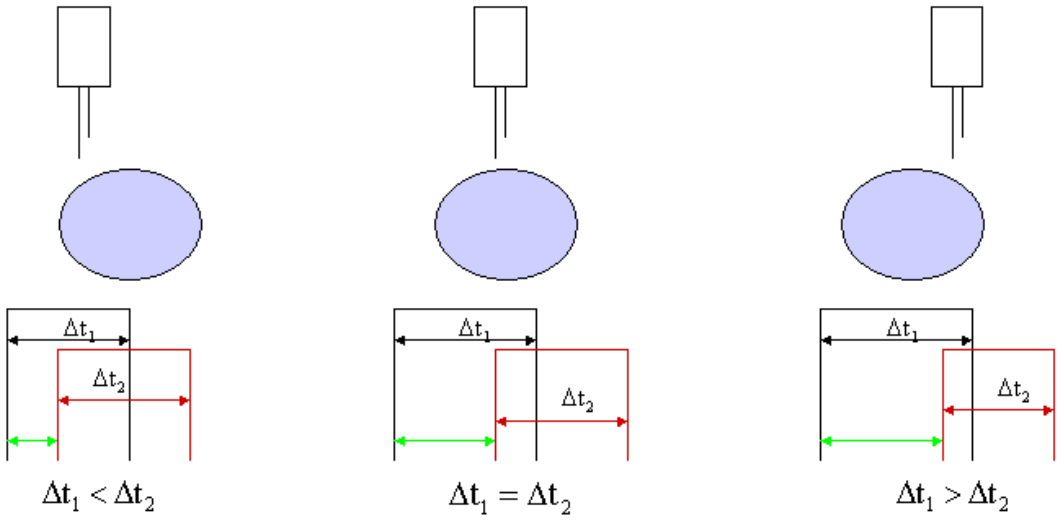

Figure 4-4: Differing strike locations.

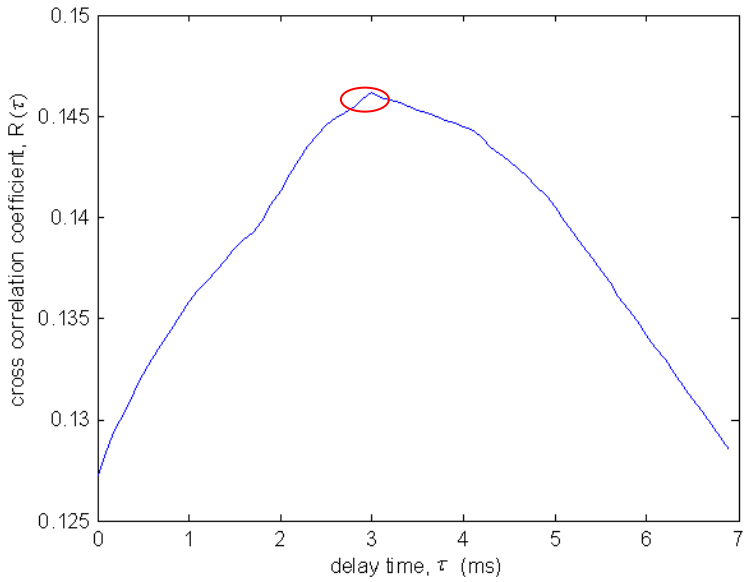

Figure 4-5: An example of typical cross correlation plot used for determining the delay time.

Dispersed-phase velocity measurements were conducted first in water-air flow and then in water-steam flow. When the air flow was slow, we could easily detect the bubbles visually from the camera and calculate the bubble velocity as described in Section 3.3.2. For slow water-air flow we obtained a good correlation between the dual optical probe and the camera-inferred velocities as can be seen in Figure 4-6.

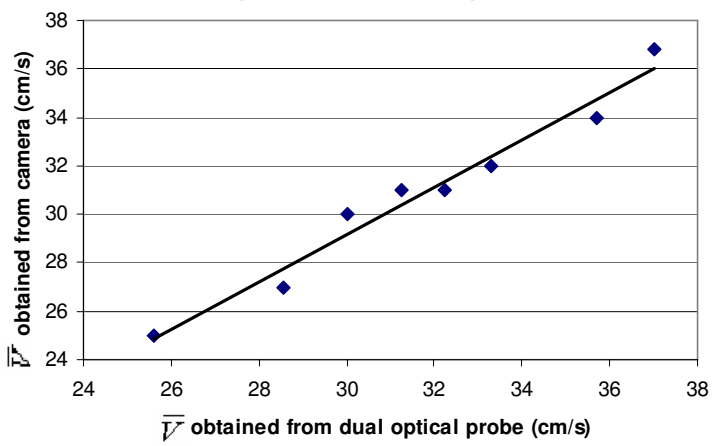

Figure 4-6: Correlation between dual optical probe and camera for slow water-air flow.

During the steam flow or fast air flow, it was hard to detect the bubbles visually from the images of the video camera as can be seen in Figure 4-7. Therefore, we could not obtain a correlation between the dual optical probe results and the video camera results, when the gas phase was flowing quickly.

Figure 4-7: Images from fast flowing gas phase.

The average dispersed-phase velocity results of the dual-optical probe for fast water-air flow and for water-steam flow were calculated by using the cross-correlation method and are tabulated in Table 4-1.

Table 4-1: Summarized results for calculated bubble flow properties for three tests.

Slow water-air flow			
Measurement Technique	**Fiber optic**	**FFRD**	**Camera**
Void Fraction (%)	28	29	-
Avg. Dispersed-Phase Velocity (cm/s)	31	-	30.5

Fast water-air flow			
Measurement Technique	**Fiber optic**	**FFRD**	**Camera**
Void Fraction (%)	61	NA	-
Avg. Dispersed-Phase Velocity (cm/s)	50	-	NA

Water-steam flow			
Measurement Technique	**Fiber optic**	**FFRD**	**Camera**
Void Fraction (%)	75	73	-
Avg. Dispersed-Phase Velocity (cm/s)	67	-	NA

As can be seen from Table 4-1 the secondary comparison methods for both void fraction and dispersed-phase velocity measurements did not give satisfactory results for fast flow rates.

4.2. Results of the Experiments in the Model Wellbore

As it was mentioned in Section *3.3.3.1* we tried three different resistivity sensor configurations. The one with copper plates measured little voltage difference for air vs. water. For the other two electrode designs, the applied voltage, smaller electrodes, and extension into the flow provided clearer and greater air vs. water differences in resistivity. Adding ions to the solution using bleach increased this effect but its quick degradation from the bubbling ruled it out for use. The four horizontally aligned electrodes performed well in a static water column with large bubbles, but in the model well they responded poorly to more intense bubbling. The vertically oriented electrodes outperformed the horizontal ones because they gave a stable rather than oscillating baseline voltage and had clearer peaks, thus the vertical configuration was preferred. Then the dual-optical probe was attached 1 cm above the vertically oriented electrodes as seen in Figure 4-8.

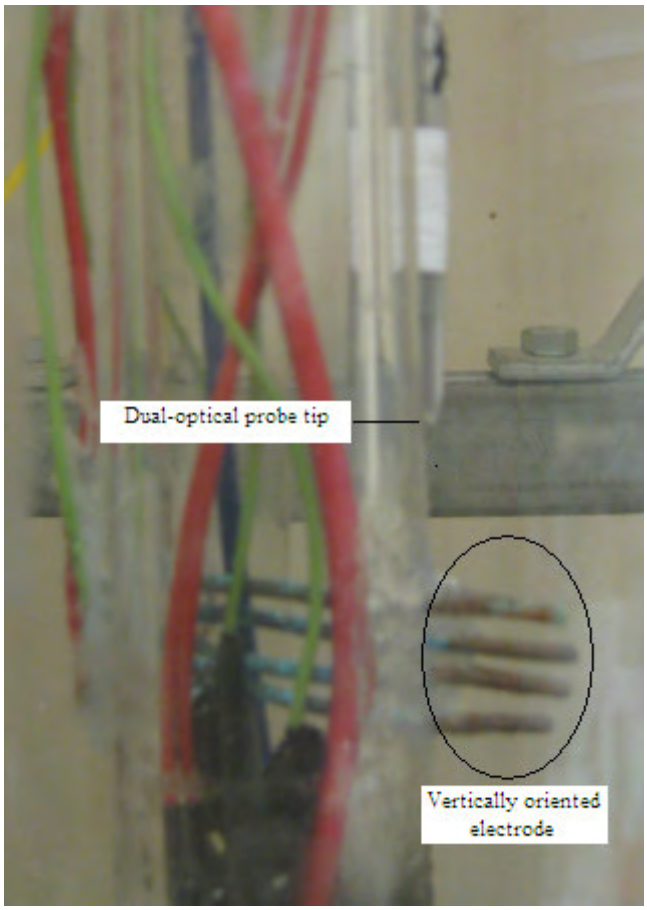

Figure 4-8: A photograph of the position of dual-optical probe and resistivity sensor.

As we mentioned in Chapter 3, resistivity-inferred and fiber-inferred average void fraction values were calculated for four different flow rates to check if there exists a correlation between these two sensors. As it can be seen in Figure 4-9, there was not a 1-1 correlation between the two sensors, since the fluid volume that the resistivity sensor was detecting was bigger than that of the fiber optic sensor.

Table 4-2: Void fraction results obtained from resistivity and fiber optic sensors for four different flow rates.

Air injection pressure (psi)	Average void fraction from resistivity sensor (%)	Average void fraction from fiber optic sensor (%)	Ratio between resistivity and fiber optic sensor results
7	4.71	1.35	3.49
10	6.15	2.67	2.31
12	6.95	3.49	1.99
20	7.46	4.09	1.83

Also we observed that with increasing air flow rate, the ratio between resistivity and fiber optic results decreased, in other words void fraction values obtained from fiber optic sensor were closer to resistivity-inferred values at high air flow rates (Table 4-2). Figure 4-10 shows typical signal patterns obtained from fiber optic and resistivity sensors, for fast and slow flow rates.

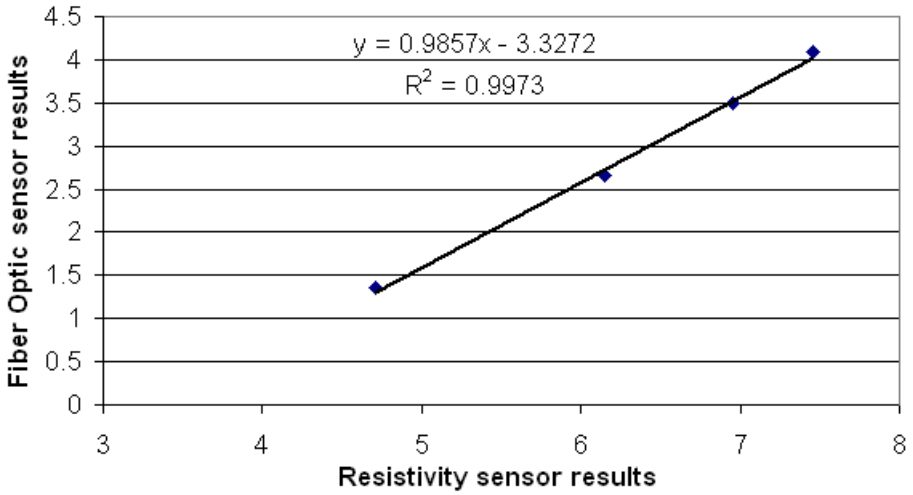

Figure 4-9: Void fraction correlation between resistivity sensor and fiber optic sensor for different air flow rates.

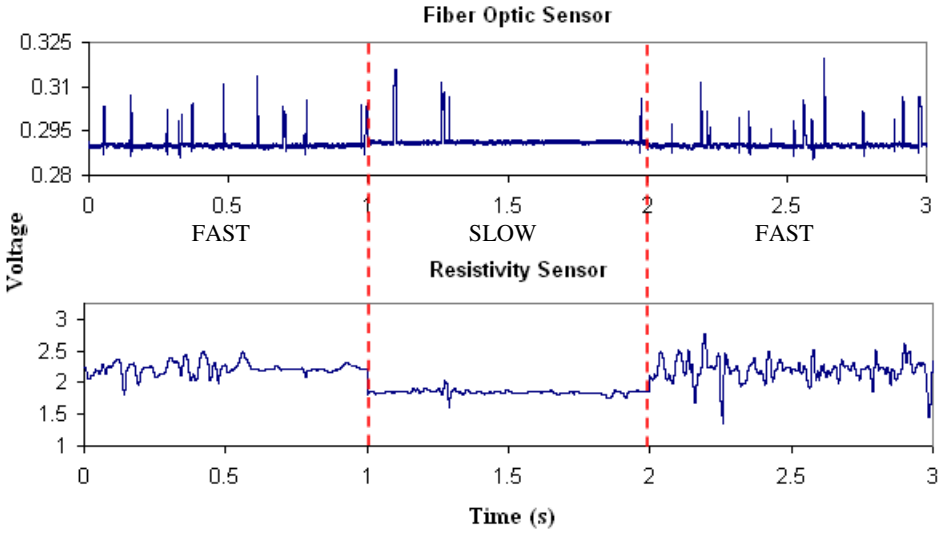

Figure 4-10: Typical fiber optic inferred and resistivity inferred signals for two different flow rates.

Chapter 5

5. Conclusion and Discussion

The set of experiments in this study has shown the applicability of the normal cut fiber optic probe for measuring local void fraction and dispersed phase velocity. These two parameters are essential factors to determine enthalpy downhole in geothermal wells.

Studies involving void fraction and dispersed phase velocity measurements by fiber optics have been reported in the literature. For instance, Morris *et al. (1987)* have shown the applicability of fiber optic probe for local void fraction measurement by using the quick closing valve technique for calibration. In addition, Hamad *et al.* (1997) obtained successful results for both void fraction and drop velocity measurements with a dual optical probe, within liquid-liquid two-phase flow.

Our study showed that the chosen comparison measurement techniques were not applicable for fast flow rates. Therefore, for the fast flow case we could not compare the fiber optic results with the FFRD, the camera or the resistivity results. Satisfactory results were obtained in the slow flow case. The fiber optic probe also appeared to be working well in fast flows, however we did not have a successful secondary measurement to confirm this.

Future work includes designing a fiber optical tool for void fraction and dispersed phase velocity measurement applicable to downhole conditions.

Nomenclature

Variables:

A = area [m^2]

α = void fraction [-]

Δx = distance between the sensor tips

Δt = bubble's travel time between two sensor tips

$\varnothing_i$ = angle of incidence or refraction

h = enthalpy per unit mass [kJ/kg]

M = dispersed phase density function

n = refraction index

p = pressure [Pa]

q = volumetric flow rate [m^3/s]

$R(\tau)$ = cross correlation function

ρ = density [kg/m^3]

S_i = measurement signal from sensor i [V (usually)]

T = total test duration [s]

t = time [s]

τ = time shift or dummy variable for time [s]

u = velocity [m/s]

U = internal energy per unit mass [kJ/kg]

V = voltage [V]

v = specific volume, volume per unit mass [m^3/kg]

W = mass flow rate [kg/s]

x = vapor phase mass fraction [-]

Subscripts:

b = bubble

g = gas or vapor phase

l = liquid phase

s = steam

w = water

0 = surrounding fluid

References

Cartellier, A., 1990 “Optical Probes for Local Void Fraction Measurements: Characterization of Performance”, *American Institute of Physics,* 61 (2), 874-886.

Cartellier, A., 1992. “Simultaneous Void Fraction Measurement, Bubble Velocity and Size Estimate using a Single Optical Probe in Gas-liquid Two-Phase Flows,” *Review of Scientific Instruments*, Vol. 63, p. 5442-5453

Chen C., R.N. Horne, M. Fourar, 2004. “Experimental Study of Two-Phase Flow Structure Effects on Relative Permeabilities in a Fracture”, *Stanford Geothermal Workshop.*

Fordham, E.J., C.P. Lenn, A. Holmes, S. Simonian, S.M. Huang and R.T. Ramos, 1999. “Multi-phase-fluid Discrimination with Local Fibre-optical Probes: I. Liquid/liquid Flows,” *Meas. Science and Technology*, Vol. 10, p. 1329-1337.

Fordham, E.J., C.P. Lenn, A. Holmes, S. Simonian, S.M. Huang and R.T. Ramos, 1999. “Multi-phase-fluid Discrimination with Local Fibre-Optical Probes: II. Gas/liquid Flows,” *Measurement Science and Technology*, Vol. 10, p. 1338-1346.

Hamad, F.A., Imberton, F., Bruun, H.H., 1997 “An Optical Probe for Measurements in Liquid-Liquid Two-phase Flow”, *Meas. Sci. Technol.,* 8, 1122-1132.

Hamad, F.A., Pierscionek, B.K., Bruun, H.H., 2000 “A Dual Optical Probe for Volume Fraction, Drop Velocity and Drop Size Measurements in Liquid-Liquid Two-phase Flow”, *Meas. Sci. Technol.,* 11, 1307-1318.

Horne, R.N.: "Geothermal Energy Assessment", in *Geothermal Reservoir Engineering*, editor E. Okandan, Reidel 1988.

Ishii, M., “Thermo-Fluid Dynamic Theory of Two Phase Flow”, in (Eyrolles, Paris, 1975), pp. 60-67.

Juliusson, E., Horne, R.N., 2006 “Downhole Enthalpy Measurement in Geothermal Wells”, *Stanford Geothermal Workshop.*

Kumar, M., Horne, R.N., 1995 *"Ultrasonic Rate Measurements in Two-Phase Bubble Flow",* SPE 30596, presented at the 70th Annual Technical Conference & Exhibition, Dallas, TX, October 22-25.

Morris, D., Teyssedou, A., Lapierre, J., Altan, T., 1987 "Optical Fibre Probe to Measure Local Void Fraction Profiles" *Appl Opt*., 26, 4660-4664.

Spielman, P., 2003. "Continuous Enthalpy Measurement of Two-Phase Flow from a Geothermal Well," *Transactions: Geothermal Resource Council 2003 Annual Meeting, October 12-15, 2003, Morelia, Mexico; GRC Transactions*, Vol. 27, p. 413-416.

Vince, M.A., H. Breed, G. Krycuk, and R.T. Lahey, 1982. "Optical Probe for High-Temperature Local Void Fraction Determination," *Applied Optics,* Vol. 21, No. 5, p.886-892.

Appendix

A. Cross Correlation Method MATLAB Code

```
%Program to calculate the cross-correlation coefficient
%for different time values. The value of tao which gives the
%maximum value for the cross-correlation coefficient (R) would
%be used to calculate the dispersed-phase velocity.
%E1 and E2 values correspond to voltage values of the
%two fibers and they should be imported from labview.
E1 = [];
E2 = [];
%Below tao range is in number of data points,
%range can be different for different tests.
tao = (1:1:70);
s = 0;
for i= 1:length(tao)
    for j= 1:length(E1)
        for n=length(E1)+1:tao(i)+length(E1)
            E2(n)=0;
        end
        s=s+(E1(j)*E2(j+tao(i)));
    end
    s=s/m;
    %m is the number of data points, it might
    %be different for different runs.
    R(i)=s;
    s=0;
end
%The range for tao can be modified depending on the input data.
%Below tao range is in millisecond.
tao=(0:0.1:6.9);
plot(tao,R)
```